Regulation of quantal currents determines synaptic strength at neuromuscular synapses in larval Drosophila

Regulation of quantal currents determines synaptic strength at neuromuscular synapses in larval *Drosophila*.

Andrew S. Powers[1], Jeffrey Grizzaffi[1], Richard Ribchester[2] and Gregory A. Lnenicka[1]

[1]Department of Biological Sciences, University at Albany, SUNY, Albany NY 12222, USA.

[2]Euan MacDonald Centre for MND Research and Centre for Cognitive and Neural Systems, University of Edinburgh, 1 George Square, Edinburgh EH8 9JZ, UK

Corresponding author: Gregory Lnenicka

Department of Biological Sciences

University at Albany, SUNY

Albany NY 12222

Email: gregL@albany.edu

Voice: 518-591-8812

Fax: 518-442-4767

ABSTRACT

Studies of synaptic homeostasis during muscle fiber (MF) growth in *Drosophila* larvae have focused on the regulation of the quantal content of transmitter release. However, early studies in crayfish and frog suggested that regulation of quantal current size may be an integral mechanism in synaptic homeostasis. To examine this further in *Drosophila*, we compared the electrical properties, minEPSPs and minEPSCs in different-sized MFs in third-instar larvae and for a single MF during larval growth. The third-instar MFs showed differences in input resistance due to differences in size and specific membrane resistance. We found that electrical coupling between MFs did not contribute substantially to the electrical properties; however, the electrode leak conductance and a slower developing increase in membrane conductance can influence the electrical recordings from these MFs. Our results demonstrated that larger MFs had larger minEPSCs to compensate for changes in MF electrical properties. This was most clearly seen for MF4 during larval growth from the second to third instar. During a predicted 80% decrease in MF input resistance, the minEPSCs showed a 35% increase in amplitude and 165% increase in duration. Simulations demonstrated that the increase in minEPSC size resulted in a 129% increase in minEPSP amplitude for third-instar larvae; this was mainly due to the increase in minEPSC duration. We also found that MFs with common innervation had similar-sized minEPSCs suggesting that MF innervation influences minEPSC size. Overall, the results showed that increased quantal content and quantal current size contribute equally to synaptic homeostasis during MF growth.

KEYWORDS: synapse, homeostasis, Drosophila, neuromuscular junction

INTRODUCTION

The matching of synaptic currents to changing postsynaptic electrical properties is an adaptive requirement for peripheral and central synapses during growth. Much of our knowledge of synaptic adaptations and homeostasis during growth has come from studies of the neuromuscular junction (NMJ) in vertebrates and invertebrates. Early studies showed that the release of more vesicles of transmitter (greater quantal content) at the NMJ contributed to the maintenance of EPSP amplitude (synaptic homeostasis) during growth of muscle fibers (MFs) in the lobster and crayfish [7;25]. In addition, compensatory differences in quantal content were reported for different-sized MFs in adult vertebrate muscle: NMJs on larger MFs had greater quantal content than those on smaller MFs [14;21]. The quantal content increase during growth was dependent upon enlargement of the MF since reducing MF growth reduced the increase in quantal content [25]. Later studies in *Drosophila* larvae demonstrated that the quantal content increase was a direct response to decreased synaptic strength; decreasing postsynaptic receptor density or muscle membrane resistance during MF growth enhanced the quantal content increase [4;9;27;29]. The mechanisms responsible for this retrograde control of transmitter release have been extensively studied at the *Drosophila* larval NMJ [6].

The contribution of changes in the synaptic current produced by individual vesicles of transmitter (quantal currents) to synaptic homeostasis at the *Drosophila* larval NMJ has not been explored although there is evidence for this in other systems. During MF growth in the crayfish, there was approximately a three-fold increase in the amplitude and duration of miniature excitatory postsynaptic currents (minEPSCs), which partially compensated for the decrease in MF input impedance [24]. In adult snake muscle, quantal current amplitude was correlated with MF size [39]. The *Drosophila* larval NMJ is a well-defined and accessible system for

quantifying changes in quantal currents; it contains identified MFs with stereotypic innervation by glutamatergic synapses. The short, isopotential MFs facilitate voltage-clamp analysis of synaptic currents; however, quantal currents have not previously been compared at different MFs in third-instar larvae, nor have they been followed at a single MF during larval growth.

Here we tested the hypothesis that adaptive mechanisms at glutamatergic neuromuscular synapses in *Drosophila* larvae regulate quantal current. To examine this, we compared the electrical properties, miniature excitatory postsynaptic potentials (minEPSPs) and minEPSCs for four different-sized MFs in third-instar larvae. In addition, the minEPSCs were examined for an identified MF during growth from a second to third-instar larvae. Modeling studies were performed to quantify the contribution of changes in quantal currents to synaptic homeostasis. We find clear evidence that an increase in minEPSC size plays a prominent role in synaptic homeostasis during MF growth.

METHODS

Experiments were performed on MFs 4, 5, 6 and 7 in segments 3 and 4 of second-instar or wandering third-instar Canton-S (CS) *Drosophila* female larvae. We distinguished second and third-instar larvae by their size and the dentation of their mouthhooks [2]. To access the NMJs, the larvae were pinned out in a physiology chamber and after an incision through the dorsal body wall, the internal organs were removed to expose the body-wall muscles. Then the segmental nerves were cut and the brain was removed. For current-clamp experiments and recording minEPSPs, we used HL3.1 saline [12] with 1.5 mM Ca^{2+}. HL3 saline [38] containing 1 mM Ca^{2+} was used for voltage-clamp experiments since the noise levels appeared lower in this saline;

this was apparently due to a higher membrane resistance in this saline. All experiments were performed at room temperature (20^{o} C).

Electrophysiology. We recorded spontaneous minEPSPs or minEPSCs using sharp microelectrodes (10–30 MΩ filled with 3 M KCl) connected to Axoclamp 2A or GeneClamp 500 (Molecular Devices, Sunnyvale, CA). Higher resistance electrodes were used for recording minEPSPs and electrical properties; lower resistance electrodes were used for recording minEPSCs using two-electrode voltage clamp. In these experiments we never observed spontaneous nerve activity resulting in evoked transmitter release. Data were acquired (sampling rate 10 kHz) using a Digidata 1440A digitizer (Molecular Devices) and pCLAMP 10.3 software (Molecular Devices). Input resistance (R_{in}) was measured in current clamp with a single electrode and the electrode resistance was digitally subtracted. The inter-segmental coupling resistance between MFs was measured by recording from MFs in adjacent segments during alternate current injections. The coupling resistance was calculated as in a previous study [1]. For two-electrode voltage clamping, the current electrode was surrounded by a grounded shield to reduce capacitive coupling and the holding potential was set at -60 mV.

We observed a change in RMP and R_{in} after penetrating some of the MFs. This was examined by measuring the RMP and R_{in} every 30 sec for 5 min. after inserting the electrodes. After 5 min., changes were observed for MF4 (n= 9), 5 (n=13) and 7 (n=12), but not for MF6 (n=12). MF4 and 5 showed a significant increase in the RMP and there was a significant decrease in the R_{in} for MF5 and 7 ($p< 0.05$; paired t-test). The increase in RMP first appeared to represent increased membrane-electrode sealing resulting in an increase in electrode shunt resistance (R_{sh}); however, this seemed unlikely since we observed decreases in R_{in}. Thus, the

slow increase in RMP appeared to result from the activation of a membrane conductance. We found that there was no change in R_{in} or RMP during the first minute after penetrating the MFs; therefore, all measurements of electrical properties and minEPSPs were performed during this first minute

Data Analysis. Spontaneous miniature events were identified using MiniAnalysis (Synaptosoft); the minEPSCs were aligned by their half-rise time and each data point was averaged. These averaged traces were analyzed in SigmaPlot 12.3 (SPSS, Plover, WI) to determine their amplitude and decay time constant (τ_{decay}). We used averaged traces for measurements since the automated measurements of single events provided by MiniAnalysis were greatly influenced by the noise levels. A previous study found that these minEPSCs often show a shoulder before the exponential decay phase due to prolonged glutamate release resulting from slow dilation of the vesicle fusion pore [28]. Therefore, we measured the minEPSC τ_{decay} by fitting an exponential function to the decay beginning at the half-amplitude as in a previous study [15]. The mean values are presented as mean ±standard error.

Calculation of electrical properties and modeling of minEPSPs. The specific membrane resistance (R_m) and specific membrane capacitance (C_m) were estimated from the equations: $R_m = (R_{in})$(total SA) and $C_m = \tau_m/R_m$. The dorsal surface area (SA) of the MF was measured and doubled to give the total surface area (total SA); this provided a good estimate of the total SA since MFs are flat (MF width/thickness was typically 4-5) with tapered edges. R_{in} was measured by applying a series of 600 ms hyperpolarizing current pulses in 1 nA increments; R_{in} was calculated for hyperpolarizations less than 40 mv and averaged to give a single value. Note that

the IV curve was almost linear in this range; e.g., hyperpolarizations 30-40 mV gave a R_{in} 10% greater than hyperpolarizations of 0-10 mV for MF6 (n= 25). The membrane time constant (τ_m) was determined by fitting an exponential curve to the voltage decay using pCLAMP 10.3 software.

We used Virtual Cell software [31;34] to model the generation of minEPSPs using a single-compartment model with membrane reactions describing the currents resulting from the synaptic and resting conductances as in our previous study [13]. The time course of the synaptic conductance (G_{syn}) was simulated using the equation: $G_{syn} = K(e^{-t/\tau 2} - e^{-t/\tau 1})G_{syn\ peak}$; where K is a scaling constant, τ_1 is the rise time constant, τ_2 is the decay time constant, and $G_{syn\ peak}$ is the peak G_{syn} [19]. $G_{syn\ peak}$ was calculated from the minEPSCs amplitude using a reversal potential of -1 mV [18]. Values for K, τ_1, and τ_2 were chosen to give the best fit to the minEPSC waveform. This Virtual Cell Model, minepsp, is available in the public domain at http://www.vcell.org/ under the shared username gregL.

RESULTS

Electrical properties of different-sized MFs. In third-instar larvae, we examined four MFs that showed a range of sizes and innervation patterns. MF5 and 7 are small fibers whereas MF4 and 6 are among the largest ones (Fig. 1A). Typically, larval MFs receive both an Is (small boutons) and Ib (big boutons) terminal, both produce fast synaptic transmission. MFs generally do not share their Ib innervation with other fibers but the axons supplying Is terminals innervate multiple fibers [16;23]. The adjacent MF6 and 7 are unusual since they are innervated by the same 2 axons and often the same Is and Ib terminals contact both fibers [23]. MF4 and 5 do not

share innervation with any of the four fibers. In addition, MF5 is unique receiving an Ib terminal but not an Is terminal.

We first compared the size and electrical properties of these four muscle fibers. The dorsal surface area (SA) of MF4, 5, 6 and 7 was measured (Fig. 1A). The SA of the largest muscle fibers (MF6 and 4) was about twice that of the smallest ones (MF7 and 5). We injected current into the muscle fibers and measured the R_{in} using a single electrode (Fig. 1B). In general, the smaller MFs had greater R_{in} than the larger ones as expected (Fig. 1B,C); however, the R_{in} was significantly greater for MF5 than MF7 even though they were similar in size. This points to differences in R_m, which was greater for MF4 (8.6 kΩ cm^2) and MF5 (8.7 kΩ cm^2) compared to MF6 (5.9 kΩ cm^2) and MF7 (4.7 kΩ cm^2). The greater R_m for MF4 and 5 was reflected in their longer τ_ms: MF4 and 5 had a τ_m near 35 ms., whereas, the τ_m was about 24 ms. for MF6 and 7 (Fig. 1C). The R_m and τ_m gave a C_m of 4-5 μF/cm^2 for the four fibers. In muscle, the R_m is usually underestimated and the C_m overestimated due to membrane infolding [10;17]. The electrical coupling between these larval MFs in adjacent segments could contribute to R_{in}. Nonetheless, the effect would be small since we found that the coupling resistance between adjacent fibers for MF6 and 7 was approximately 60 MΩ and it was about 140 MΩ for MF4; there was no apparent electrical coupling for MF5. The resting membrane potential (RMP) was similar for all the MFs except for MF5, which had a significantly smaller RMP (Fig. 1C).

Source of error in measuring MF electrical properties. We found that the electrical recordings from these MFs were influenced by leakage around the electrode (R_{sh}). Early studies of the frog NMJ reported a large range of R_{sh} (5-100 MΩ) with an average around 10 MΩ; this R_{sh} had minimal effect on recordings from frog twitch MFs due to their low R_{in} (< 1 MΩ) but greater

effects on the RMP and R_{in} of slow MFs, which had higher R_{in} (4-5 MΩ) [17;36]. Given the relatively high R_{in} for the larval MFs, the R_{sh} would be expected to affect these electrical recordings. We briefly examined the effect of R_{sh} by recording the R_{in} before (R_{in}^{A}) and after (R_{in}^{B}) the introduction of a second electrode in MF6. We found that penetration by a second electrode resulted in an immediate 27.0 ±4.9 % (n=7) reduction in R_{in} presumably due to the introduction of a second R_{sh}. Based upon a circuit containing the parallel resistors R_{sh} and R_{in}, R_{sh} was calculated from the equation: $R_{sh} = (R_{in}^{A})(R_{in}^{B})/(R_{in}^{A} - R_{in}^{B})$. The average R_{sh} was 33.4 ±14.7 MΩ (n= 7) and showed considerable variability; the electrode resistance for the second electrode was 20-30 MΩ. This R_{sh} would result in an underestimation of the RMP, R_{in} and R_{m}. In addition, since the effect of R_{sh} would be greater for MFs with higher R_{in}, we would expect that the differences in R_{in} and R_{m} for these MFs were greater than our values show. For RMPs, it seemed likely that MF5's relatively low RMP was due to its high R_{in}; we corrected the RMPs for the R_{sh} to explore this possibility. Based upon the equivalent circuit where the RMP battery and R_{in} are in parallel with the electrode leak battery (0 potential) and R_{sh}, the corrected RMP (RMP′) is given by the equation: $RMP' = RMP(R_{in} + R_{sh})/R_{sh}$; where RMP is the measured RMP. RMP′ for the four MFs were very similar ranging from -76.8 to -79.8 (Fig. 1C). The RMP′ should be taken as an approximation given the high variability in R_{sh}; however, it appears very likely that the RMP in MF5 is similar to that in the other MFs and our low values for MF5 were an artifact produced by R_{sh}.

Although the R_{sh} produced errors in the measurements of electrical properties and minEPSPs, it should have no effect on the conclusions of this study. The electrical properties were used to predict the properties of the minEPSPs (below) and since both were recorded under

the same conditions (similar R_{sh}) the comparisons were valid. Of course, the R_{sh} should not affect the measurement of minEPSCs.

Differences in minEPSPs in different-sized MFs. Based upon the MF's electrical properties, the predicted differences in minEPSP amplitude were modeled assuming that the G_{syn} producing the minEPSP was constant (see Methods). Based upon these simulations, we found that MF5 should have the largest minEPSPs followed by MF7, 6 and 4 (Fig. 2A). To test whether this occurred, we examined the minEPSPs in the four MFs; spontaneous minEPSPs were recorded during the first minute after penetrating the MF (Fig. 2B). The minEPSPs were averaged to give a single trace for each MF and measurements were made from the averaged trace (see Methods).

In general, we found that the relative minEPSP amplitudes were similar to the expected pattern (Fig. 2C). As predicted, the minEPSP amplitude for MF6 was 72% of that seen in MF7; however, the minEPSP amplitude for MF5 was not as large as predicted in relation to the other fibers. This observation was underscored when comparing MF5 to MF4; the minEPSP amplitude in MF4 was predicted to be 53% of that in MF5 but instead it was 80% and the difference between MF4 and 5 was not significant. The minEPSP τ_{decay} was smaller for MF6 and 7 compared to MF4 and 5; this is consistent with the differences in the τ_m for these MFs (Fig. 2C).

Comparison of minEPSCs in different-sized MFs. We examined the quantal currents in these four MFs by voltage clamping them and measuring the amplitude and duration of the spontaneously occurring minEPSCs (Fig. 3A). The minEPSCs were recorded for approximately 3 min. and averaged to give a single trace, which was used to measure the amplitude and decay.

MFs 6 and 7 had very similar minEPSCs, their amplitudes and τ_{decay}s were not significantly different (Fig. 3B,C). This was expected since the differences in their minEPSP amplitudes were similar to those predicted by their MF electrical properties assuming a constant minEPSC. The MF4 minEPSC amplitude was significantly greater than that found in MF5. Here, the larger fiber with the lower input impedance had the larger minEPSC; this was presumably responsible for the similarity in the minEPSP amplitudes for MF4 and 5.

It was surprising that MF6 and 7 had comparable minEPSCs in spite of the differences in MF size; this could be due to their shared innervation. If the innervation influences quantal current size, then we would expect that minEPSC size in the two fibers should be correlated. We analyzed experiments where we recorded minEPSCs from MF6 and 7 pairs in the same hemisegment (Fig. 4). We found that minEPSC amplitudes recorded from MF6 were strongly correlated with those found in the adjacent MF7. This suggests a role for the nerve in regulating the size of quantal currents.

minEPSC size increases during MF growth. To determine whether an increase in quantal currents contributed to synaptic homeostasis during growth, we compared MF4 minEPSCs in second and third-instar larvae. Larvae undergo considerable growth from the second to third instar and MF4 showed about a 5-fold increase in SA (Fig. 5A). It was previously found that R_m did not change during growth of crayfish MFs [24]. Assuming that R_m remains constant during growth of MF4, the projected R_{in} for MF4 in second instars was 40.2 MΩ; therefore, the R_{in} decreased by 80% during growth from a second to third instar. Note that if the effects of R_{sh} were considered, the R_{in} for both second and third instars would increase by approximately 20%. During growth, we found a large increase in minEPSC size (Fig. 5B): there was a significant

increase in both the amplitude (35%) and τ_{decay} (165%) resulting in a 252% increase in charge transfer

The effect of the increase in minEPSC size on minEPSP size was examined using simulations. In our simulations, we used the G_{syn} derived from minEPSC measurements from MF4 in second and third instar larvae (Fig. 5), values for R_m, C_m and RMP were taken from MF4 in third-instar larvae (Fig. 1) and the MF4 SAs were from second and third-instar larvae (Fig 5). According to the simulations, the minEPSP amplitude decreased from 1.64 mV in the second instar to 0.78 mV in the third instar (Fig. 6A). Note that the third-instar simulated minEPSP amplitude was very similar to our measured minEPSP amplitude (.79 mV). Their waveforms were also similar with the exception that the recorded minEPSP showed a more rapid initial decay; we do not know the reason for this discrepancy. If there was no increase in the quantal currents during growth, the minEPSP amplitude would be predicted to decrease to 0.34 mV in the third instar (Fig. 6B). The increase in quantal current contributes to homeostasis of EPSP amplitude during growth since the minEPSP amplitude in third-instar larvae was 129% greater than it would be without an increase in quantal current. Given the remaining difference between the second and third-instar minEPSP amplitudes, quantal content would need to increase by 110% to maintain a stable EPSP amplitude during growth.

The quantal current change during growth involves both increased minEPSC amplitude and duration. To compare their effects on the minEPSP, we simulated the increase in minEPSC amplitude without the increase in duration; the resultant minEPSP amplitude in third-instar MFs was 0.45 mV (Fig. 6C). Therefore, the increase in minEPSC amplitude during growth only contributed 32% to the total 129% increase in minEPSP amplitude and the increase in minEPSC duration had a greater effect on synaptic homeostasis.

DISCUSSION

MF Electrical properties and minEPSPs. We measured the electrical properties of the MFs and found that there was almost a 4-fold range of R_{in} due to differences in MF size and R_m. These differences in R_{in} and R_m were likely underestimations due to the $R_{sh.}$ Our R_{in} were generally higher than previously reported for third-instar larval muscle fibers (e.g. MF6 in [18;23]) and this was likely due to using a single electrode and making measurements soon after penetrating the fibers. During prolonged recordings, the R_{in} was often seen to decrease and the RMP increase, this was particularly true for MF5. The reduction in R_{in} and increase in RMP would be consistent with activation of a Ca^{2+}-dependent K^+ conductance; this is supported by our previous findings that activation of the *Drosophila* SK (dSK) channel is involved in generating the RMP in larval MFs [13]. The electrode leak could have the dual effect of initially reducing the RMP and R_{in} by shunting the membrane currents and subsequently activating the dSK channel by allowing Ca^{2+} influx; this would further reduce R_{in} but increase the RMP during prolonged recordings. This is similar to the effect reported when recording from neurons in the CNS with sharp electrodes [35].

The differences in MF R_{in} and τ_m were predicted to result in differences in minEPSP amplitude and decay. MF4 and 5 had minEPSP τ_{decay}s that were longer than those seen in MF6 and 7 consistent with their differences in τ_m. The predicted differences in minEPSP amplitude were also seen; however, some differences were not as great as predicted suggesting compensatory changes in minEPSC size.

Larger fibers showed a compensatory increase in minEPSC size. We recorded minEPSCs from the four MFs and measured the minEPSC amplitude and τ_{decay}. Our values for the MF6

minEPSCs were similar to previously reported ones. Voltage-clamp studies of MF6 (holding potential -70mV) gave minEPSC amplitudes of 0.5 to 0.6 nA [30;33], which is similar to our value of 0.43 nA, considering that our holding potential was -60 mV. A previous study examined the minEPSC τ_{decay} by recording synaptic currents near the MF6-7 cleft using an extracellular electrode, which provides the most reliable measure of the synaptic current waveform [15]. This gave a minEPSC τ_{decay} of 4.4 ms., which is very close to our value of 4.2 ms. for MF6.

MF4 and 5 showed the greatest difference in size and input impedance encountered by the synaptic current; i.e. they had the largest predicted difference in minEPSP amplitude assuming a constant minEPSC. We found that MF4 had a greater minEPSC amplitude than MF5; this appears to be a compensatory response to these differences in MF size and input impedance. This finding is consistent with adult snake muscle where both quantal content and quantal current amplitude were positively correlated with fiber size [39]. Alternatively, our difference in minEPSC amplitude could reflect differences in the innervation: MF4 minEPSCs arise from both Is and Ib terminals, whereas, MF5 only receives an Ib terminal. A previous study found that Is terminals had larger synaptic vesicles and produced greater amplitude minEPSCs than Ib terminals for MF6 [20;28]. If the Is and Ib terminals on MF 4 and 5 show similar differences, this could lead to a larger mean minEPSC amplitude for MF4.

To further explore the effect of MF size on minEPSC size, we examined MF4 during larval growth from a second to third-instar. During this period, the SA of MF4 increased 5-fold resulting in a large predicted decrease in the MF input impedance. Here we found clear evidence that minEPSC size is related to MF size: the minEPSCs showed a 35% increase in amplitude and 165% increase in τ_{decay} during MF growth. These results are consistent with the crayfish where

there was an increase in minEPSC amplitude and duration during MF growth [24]. Modeling was used to compare the effect of the increase in minEPSC amplitude and duration in the maintenance of minEPSP amplitude and we found that the increase in duration made a larger contribution than the increase in amplitude. However, since there was no significant difference in minEPSP τ_{decay} for MF 4 and 5 in third-instar larvae, it may be that compensatory changes in τ_{decay} are important during larval growth but not for different-sized fibers at the same larval stage. Although we only compared second and third-instar larvae, it appears likely that the increase in minEPSC size occurs throughout larval growth. minEPSCs recorded from MF6 in *Drosophila* embryos had amplitudes of about 150 pA [3;11]; this small amplitude could have been due to the immature synapses or the matching of minEPSC size to the small MFs. Based upon our results, it appears likely that these small minEPSCs were part of a continuum where minEPSC size scales with MF size throughout growth.

It was surprising to find that different-sized MFs sharing motor terminals had similar-sized minEPSCs. Even though MF6 was much larger than MF7, the minEPSC amplitude and τ_{decay} were not significantly different. In addition, the inter-animal variability in minEPSC amplitude was correlated for the two fibers. These two MFs not only share the same axons but often the same terminal branches and it appears possible that the innervation influenced minEPSC size.

Regulation of minEPSCs size as a mechanism for synaptic homeostasis. Our results showed that the increase in minEPSC size during growth from the second to third instar larvae resulted in a minEPSP amplitude that was 129% greater than expected if there was no increase in minEPSCs. To maintain a stable EPSP, an additional 110% increase in the quantal content would be

required. Thus the contribution of increased minEPSC size to synaptic homeostasis was actually slightly greater than the increase in quantal content. It has been clearly shown that an experimental reduction in synaptic strength can produce a compensatory increase in quantal content [6]. Is the increase in quantal current size also a direct response to reduced synaptic efficacy during MF growth? The evidence for this at the larval NMJ is mixed. It was reported that there was a compensatory increase in the quantal current size after an experimental reduction in the number of synaptic boutons and quantal content at larval MFs [5]; however, when synaptic strength was decreased by expressing additional MF K^+ channels, there was a compensatory increase in quantal content but no increase in quantal current amplitude [27]. It may be that both contribute to synaptic homeostasis but quantal content is more highly regulated and responsible for fine-tuning.

The simplest explanation for the increase in minEPSC amplitude and duration seen during growth would be an increase in the GluRIIA/GluRIIB subunit ratio. The larval glutamate receptors are heterotetamers that contain either one GluRIIA or one GluRIIB subunit and receptors with a GluRIIB subunit show more rapid desensitization than those with a GluRIIA subunit [8;9]. Due to these differences in desensitization, transgenic larvae with only GluRIIA subunits showed greater minEPSC amplitude and duration than those with only GluRIIB subunits [28]. An increase in the GluRIIA/GluRIIB subunit ratio was not supported by the observation that newly-formed postsynaptic densities in third-instar larvae have predominantly GluRIIA subunits and the proportion of GluRIIB subunits increased as they matured over a period of hours [32]. Nonetheless, the GluRIIA/GluRIIB subunit ratio should be compared for second and third-instar larvae.

The similar-sized minEPSCs for MFs 6 and 7 could result from their identical synaptic activity since synaptic activity has been shown to influence minEPSC size. For example, chronic stimulation of the motor nerve and muscle with channelrhodopsin-2 resulted in more GluRIIA receptors and increased minEPSC duration at the larval NMJ [22]. Also, a prolonged increase in locomotor activity resulted in an increase in minEPSP amplitude due to an increase in the size of presynaptic vesicles and presumably the amount of transmitter per vesicle [37]. Finally, synaptic activity could influence the minEPSC size by regulating the phosphorylation state of the GluRIIA subunit. The postsynaptic response to glutamate is enhanced by inhibiting protein kinase A (PKA) and reduced by activating PKA presumably due to its phosphorylation of the GluRIIA subunit [4]. Alternatively, an effect of innervation on minEPSC size could result from the structural properties of the motor terminal influencing minEPSC size; it was found that the number of postsynaptic glutamate receptors is positively correlated with the size of presynaptic active zones [26]. It may be that as the terminal expands on a growing MF, there is an increase in active zone size resulting in a change in the composition of the postsynaptic receptors; this mechanism might contribute to both the growth-related increase in minEPSC amplitude and a possible influence of the nerve on minEPSC size.

FIGURE LEGENDS

Figure 1. Differences in size and electrical properties of larval MFs. *A:* An image of a hemisegment in a third-instar larva showing MF7, 6, 5 and 4 (outlined with white stippled line). This tissue was fixed and the terminals stained using an antibody to HRP; the muscles were viewed with DIC to emphasize the MFs and not the terminals. Measurements of the MF SA showed that MF6 and 4 were significantly larger than MF7 and 5. The number of MFs measured appears on the bars and the x-axis gives the identity of the MF. The total number of larvae was 15. *B:* Representative current injection for MF5 and 6. The same current injection (I) produced a much greater change in membrane voltage (V) in MF5 compared to MF6. Calibration: V- 10 mV, 200 ms; I- 2 nA, 200 ms. *C:* The mean electrical values for the four MFs. The MF R_{in} was greatest for MF5 followed by MF7. The τ_m was greatest for MF5 and 4. The measured MF5 RMP was significantly lower than all the other MF RMPs; however, the corrected RMPs (●) based upon an R_{sh} of 33.4 MΩ were similar for all the MFs. The total number of larvae was 18. Statistical analysis was performed using one-way ANOVA with post-hoc Bonferroni t-test: *$p < 0.05$; **$p < 0.01$; ***$p < 0.001$.

Figure 2. minEPSPs for MF7, 6, 5 and 4. *A:* The MF electrical properties were used to predict the relative minEPSP amplitudes assuming that the G_{syn} producing the minEPSP was the same for all MFs. Values were normalized to the predicted minEPSP amplitude for MF5. *B:* The averaged minEPSPs for the four different MFs are shown; all the minEPSPs were averaged to give a single trace. *C:* Mean values for the minEPSP amplitude and τ_{decay} are shown. The number of MFs measured appears on the bars and the x-axis gives the identity of the MF. The

total number of larvae was 8. Statistical analysis was performed using one-way ANOVA with post-hoc Bonferroni t-test: *p < 0.05; **p < 0.01; ***p < 0.001.

Figure 3. minEPSCs recorded from the four MFs. *A:* Representative spontaneous minEPSCs recorded from MF5 and 4. The larger MF4 generally had larger minEPSCs. Note that MF4 sometimes had a population of small, slow minEPSCs (asterisk), which apparently originated in MF4 in the adjacent segment. These distant minEPSCs were easily distinguished from the ones originating in the targeted MF and were not included in the measurements. *B:* Traces representing the average of all minEPSCs show that minEPSCs for MF6 and 7 were very similar; whereas, MF4 minEPSCs were larger those in MF5. *C:* Quantification of the differences in minEPSCs for the four fibers. The number of MFs measured appears on the bars and the x-axis gives the identity of the MF. The (mean frequency) and mean number of minEPSCs averaged for each MF were: MF7- (0.4 ±0.1 Hz) 69 ±19; MF6- (1.0 ±0.3 Hz) 222 ±68; MF5- (0.4 ±0.1 Hz) 62 ±7 and MF4- (1.1 ±0.1 Hz) 197 ±21. The total number of larvae was 24. Statistical analysis was performed using one-way ANOVA with post-hoc Bonferroni t-test: *p < 0.05; **p < 0.01.

Figure 4. minEPSC amplitude is correlated in paired MF6 and 7. *A:* Representative traces of minEPSCs recorded from MF6 and 7 pairs. The minEPSC traces were averages from each MF. Note that these traces show their digitization; this is not seen for other minEPSCs since they are the average of many individual MF traces. *B:* The minEPSC amplitudes recorded from MF pairs were significantly correlated (p< .01). The total number of larvae was 10.

Figure 5. minEPSCs during growth of MF4. *A:* Representative MF4s in second and third-instar larvae. MF4 is outlined (white stippled line) in DIC images from live tissue. The bar graph shows that the mean MF SA is about 5 times greater in third-instar larvae compared to second instars. The total number of larvae was 25. *B:* The averaged minEPSCs show that their amplitude and duration were greater in third-instar larvae compared to second instars. The traces are the average of the minEPSCs from all the MFs. *C:* MF4 minEPSC measurements from second and third-instar larvae. The minEPSC amplitude and τ_{decay} were significantly greater in third-instar larvae compared to second instars. The number of MFs is given on the bars and the total number of larvae was 17. The (mean frequency) and mean number of minEPSCs averaged for each fiber were: 2nd instar- (0.1 ±0.02 Hz) 23 ±9; 3rd instar- (1.1 ±0.1 Hz) 197 ±21. Second and third-instar larvae were compared with a t-test: ** $p < .01$; *** $p < .001$.

Figure 6. Modelling of MF4 minEPSCs and minEPSPs. *A.* Although the minEPSC size increased during growth from a second (2nd instar) to third instar (3rd instar) larvae, there was still a decrease minEPSP amplitude due to the large decrease in input impedance. For the third-instar larvae, the recorded minEPSP from Fig. 2 (gray trace) was superimposed on the simulated minEPSP. *B.* The minEPSP in third-instar larvae was simulated assuming no increase in minEPSC size. This minEPSP was much smaller than found in third-instar larvae (*A: 3rd instar*) demonstrating the compensatory effect of the increase in minEPSC size. *C.* When the minEPSC had a third-instar amplitude and second-instar duration, the minEPSP amplitude seen in a third-instar MF was only slightly larger than that seen in *B*.

REFERENCES

1. Bennett MV (1966) Physiology of electrotonic junctions. Ann N Y Acad Sci 137:509-539

2. Bodenstein D (1950) The Postembryonic Development of Drosophila. In: Demerec M (ed) Biology of Drosophila. first edn. John Wiley & Sons, Inc., New York, pp 275-367

3. Daniels RW, Collins CA, Chen K, Gelfand MV, Featherstone DE, DiAntonio A (2006) A single vesicular glutamate transporter is sufficient to fill a synaptic vesicle. Neuron 49:11-16

4. Davis GW, DiAntonio A, Petersen SA, Goodman CS (1998) Postsynaptic PKA controls quantal size and reveals a retrograde signal that regulates presynaptic transmitter release in Drosophila. Neuron 20:305-315

5. Davis GW, Goodman CS (1998) Synapse-specific control of synaptic efficacy at the terminals of a single neuron. Nature 392:82-86

6. Davis GW, Muller M (2015) Homeostatic control of presynaptic neurotransmitter release. Annu Rev Physiol 77:251-70.

7. DeRosa RA, Govind CK (1978) Transmitter output increases in an identifiable lobster motoneurone with growth of its muscle fibres. Nature 273:676-678

8. DiAntonio A (2006) Glutamate receptors at the Drosophila neuromuscular junction. Int Rev Neurobiol 75:165-79.

9. DiAntonio A, Petersen SA, Heckmann M, Goodman CS (1999) Glutamate receptor expression regulates quantal size and quantal content at the Drosophila neuromuscular junction. J Neurosci 19:3023-3032

10. Dulhunty AF, Franzini-Armstrong C (1975) The relative contributions of the folds and caveolae to the surface membrane of frog skeletal muscle fibres at different sarcomere lengths. J Physiol 250:513-539

11. Featherstone DE, Rushton E, Broadie K (2002) Developmental regulation of glutamate receptor field size by nonvesicular glutamate release. Nat Neurosci 5:141-146

12. Feng Y, Ueda A, Wu CF (2004) A modified minimal hemolymph-like solution, HL3.1, for physiological recordings at the neuromuscular junctions of normal and mutant Drosophila larvae. J Neurogenet 18:377-402

13. Gertner DM, Desai S, Lnenicka GA (2014) Synaptic excitation is regulated by the postsynaptic dSK channel at the Drosophila larval NMJ. J Neurophysiol 111:2533-2543

14. Harris JB, Ribchester RR (1979) The relationship between end-plate size and transmitter release in normal and dystrophic muscles of the mouse. J Physiol 296:245-65.

15. Heckmann M, Dudel J (1998) Evoked quantal currents at neuromuscular junctions of wild type Drosophila larvae. Neurosci Lett 256:77-80

16. Hoang B, Chiba A (2001) Single-cell analysis of Drosophila larval neuromuscular synapses. Dev Biol 229:55-70

17. Hodgkin AL, Nakajima S (1972) The effect of diameter on the electrical constants of frog skeletal muscle fibres. J Physiol 221:105-120

18. Jan LY, Jan YN (1976) Properties of the larval neuromuscular junction in Drosophila melanogaster. J Physiol 262:189-214

19. Johnston D, Wu SM (1995) Foundations of Cellular Neurophysiology. The MIT Press, Cambridge MA

20. Karunanithi S, Marin L, Wong K, Atwood HL (2002) Quantal size and variation determined by vesicle size in normal and mutant Drosophila glutamatergic synapses. J Neurosci 22:10267-10276

21. Kuno M, Turkanis SA, Weakly JN (1971) Correlation between nerve terminal size and transmitter release at the neuromuscular junction of the frog. J Physiol 213:545-556

22. Ljaschenko D, Ehmann N, Kittel RJ (2013) Hebbian plasticity guides maturation of glutamate receptor fields in vivo. Cell Rep 3:1407-1413

23. Lnenicka GA, Keshishian H (2000) Identified motor terminals in Drosophila larvae show distinct differences in morphology and physiology. J Neurobiol 43:186-197

24. Lnenicka GA, Mellon D, Jr. (1983) Changes in electrical properties and quantal current during growth of identified muscle fibres in the crayfish. J Physiol 345:261-284

25. Lnenicka GA, Mellon D, Jr. (1983) Transmitter release during normal and altered growth of identified muscle fibres in the crayfish. J Physiol 345:285-296

26. Marrus SB, DiAntonio A (2004) Preferential localization of glutamate receptors opposite sites of high presynaptic release. Curr Biol 14:924-931

27. Paradis S, Sweeney ST, Davis GW (2001) Homeostatic control of presynaptic release is triggered by postsynaptic membrane depolarization. Neuron 30:737-749

28. Pawlu C, DiAntonio A, Heckmann M (2004) Postfusional control of quantal current shape. Neuron 42:607-618

29. Petersen SA, Fetter RD, Noordermeer JN, Goodman CS, DiAntonio A (1997) Genetic analysis of glutamate receptors in Drosophila reveals a retrograde signal regulating presynaptic transmitter release. Neuron 19:1237-1248

30. Sandstrom DJ (2004) Isoflurane depresses glutamate release by reducing neuronal excitability at the Drosophila neuromuscular junction. J Physiol 558:489-502

31. Schaff J, Fink CC, Slepchenko B, Carson JH, Loew LM (1997) A general computational framework for modeling cellular structure and function. Biophys J 73:1135-1146

32. Schmid A, Hallermann S, Kittel RJ, Khorramshahi O, Frolich AM, Quentin C, Rasse TM, Mertel S, Heckmann M, Sigrist SJ (2008) Activity-dependent site-specific changes of glutamate receptor composition in vivo. Nat Neurosci 11:659-666

33. Sigrist SJ, Thiel PR, Reiff DF, Lachance PE, Lasko P, Schuster CM (2000) Postsynaptic translation affects the efficacy and morphology of neuromuscular junctions. Nature 405:1062-1065

34. Slepchenko BM, Schaff JC, Macara I, Loew LM (2003) Quantitative cell biology with the Virtual Cell. Trends Cell Biol 13:570-576

35. Staley KJ, Otis TS, Mody I (1992) Membrane properties of dentate gyrus granule cells: comparison of sharp microelectrode and whole-cell recordings. J Neurophysiol 67:1346-1358

36. Stefani E, Steinbach AB (1969) Resting potential and electrical properties of frog slow muscle fibres. Effect of different external solutions. J Physiol 203:383-401

37. Steinert JR, Kuromi H, Hellwig A, Knirr M, Wyatt AW, Kidokoro Y, Schuster CM (2006) Experience-dependent formation and recruitment of large vesicles from reserve pool. Neuron 50:723-733

38. Stewart BA, Atwood HL, Renger JJ, Wang J, Wu CF (1994) Improved stability of Drosophila larval neuromuscular preparations in haemolymph-like physiological solutions. J Comp Physiol [A] 175:179-191

39. Wilkinson RS, Lunin SD, Stevermer JJ (1992) Regulation of single quantal efficacy at the snake neuromuscular junction. J Physiol 448:413-36.:413-436

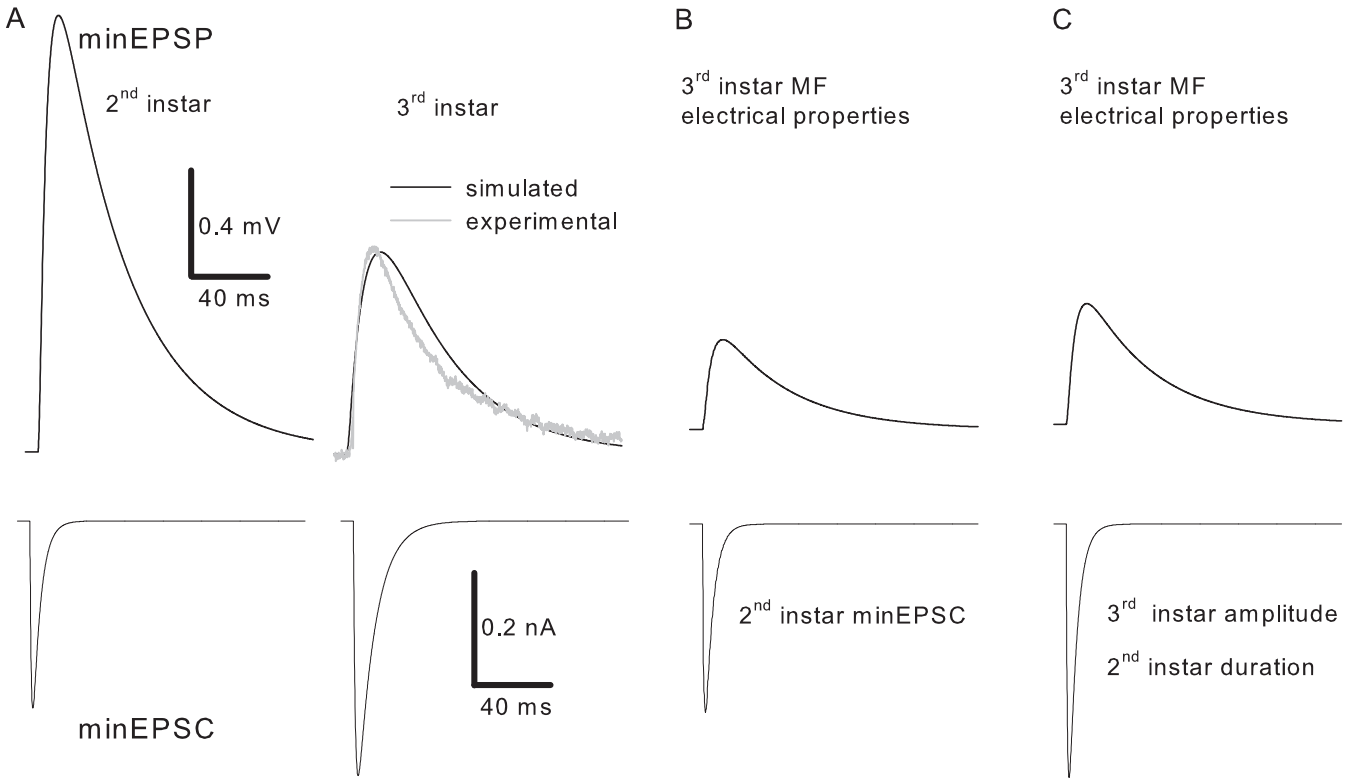
A
minEPSP
2nd instar
0.4 mV
40 ms
3rd instar
simulated
experimental
minEPSC
0.2 nA
40 ms
B
3rd instar MF
electrical properties
2nd instar minEPSC
C
3rd instar MF
electrical properties
3rd instar amplitude
2nd instar duration

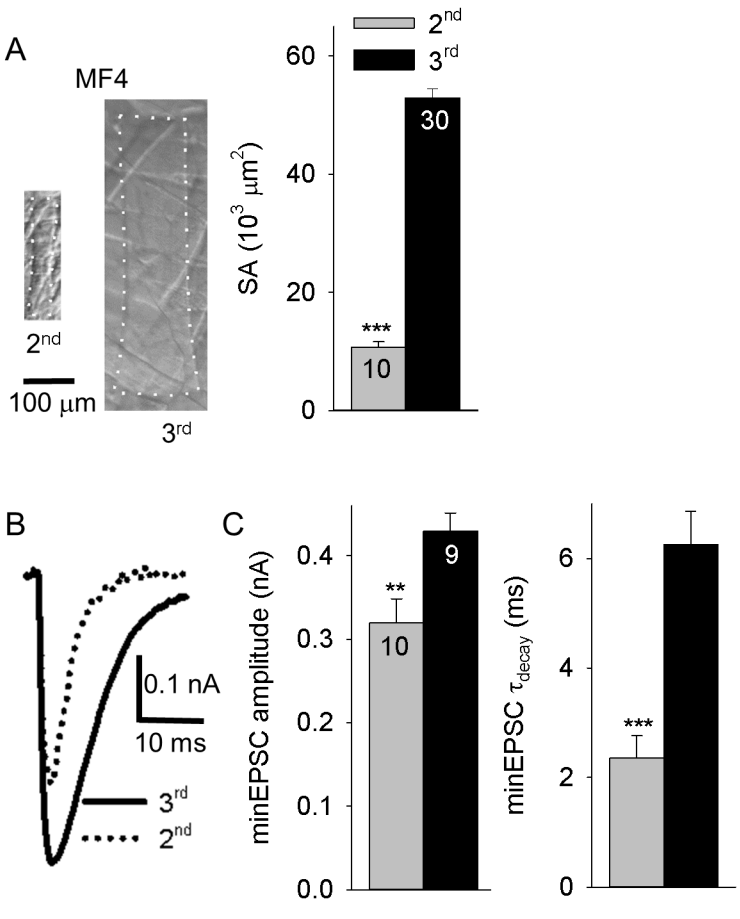
A
MF4
2nd
100 μm
3rd
2nd
3rd
SA (10^3 μm^2)
60
40
20
0
***
10
30
B
0.1 nA
10 ms
3rd
2nd
C
minEPSC amplitude (nA)
0.4
0.3
0.2
0.1
0.0
**
10
9
minEPSC τdecay (ms)
6
4
2
0
***

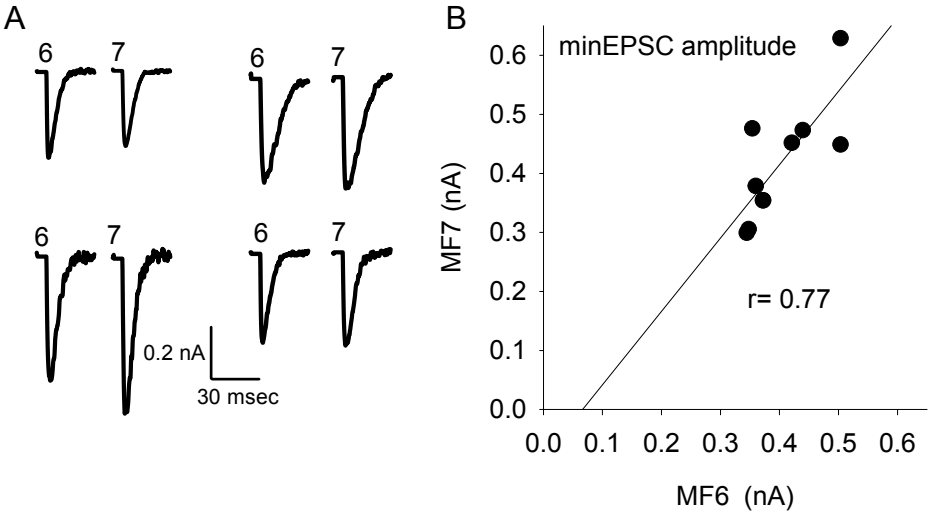
A
6
7
6
7
6
7
6
7
0.2 nA
30 msec
B
minEPSC amplitude
MF7 (nA)
0.0
0.1
0.2
0.3
0.4
0.5
0.6
r= 0.77
0.0
0.1
0.2
0.3
0.4
0.5
0.6
MF6 (nA)

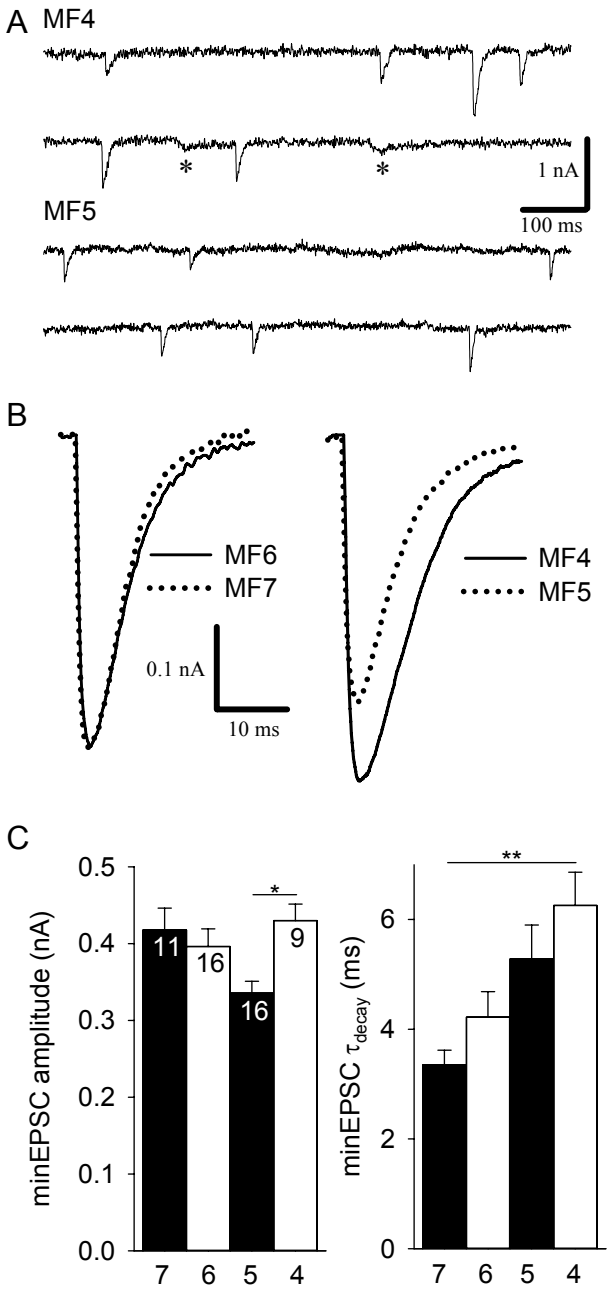
A
MF4
1 nA
100 ms
MF5
B
MF6
MF7
0.1 nA
10 ms
MF4
MF5
C
minEPSC amplitude (nA)
0.5
0.4
0.3
0.2
0.1
0.0
11
16
16
9
*
7 6 5 4
minEPSC τdecay (ms)
**
6
4
2
0
7 6 5 4

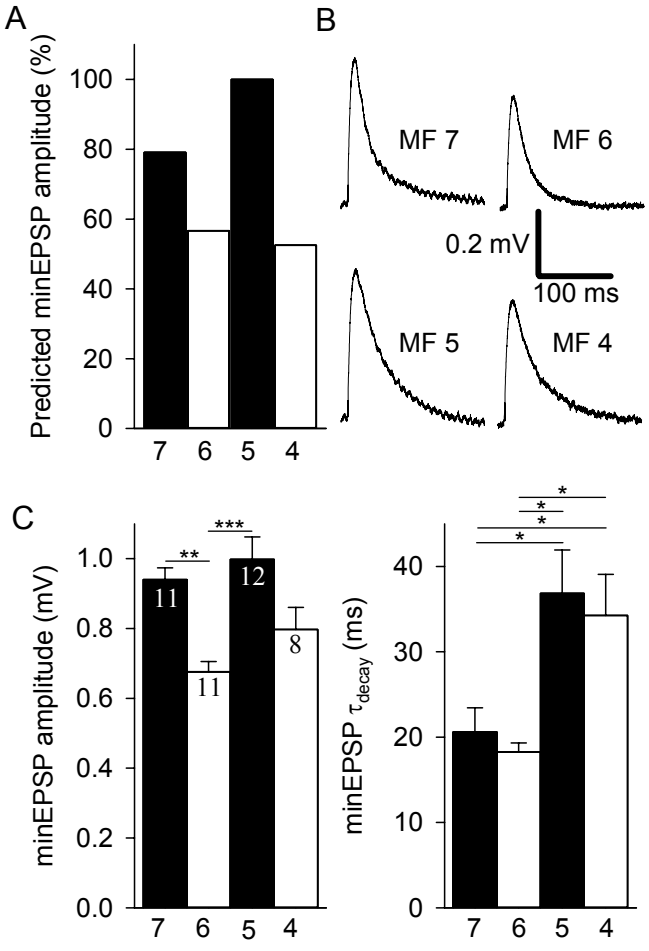
A
B
Predicted minEPSP amplitude (%)
100
80
60
40
20
0
7 6 5 4
MF 7
MF 6
0.2 mV
100 ms
MF 5
MF 4
C
minEPSP amplitude (mV)
1.0
0.8
0.6
0.4
0.2
0.0
**
***
11
11
12
8
7 6 5 4
minEPSP τ_{decay} (ms)
40
30
20
10
0
*
*
*
*
7 6 5 4

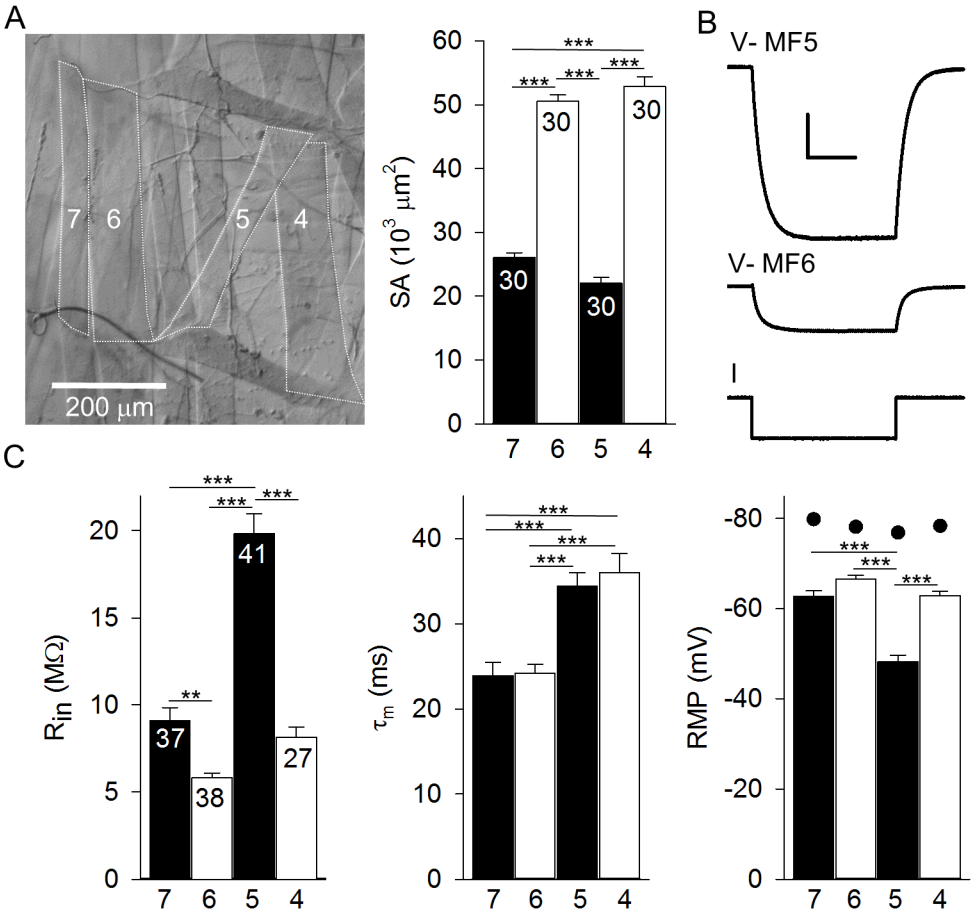
A
7
6
5
4
200 µm
SA (10^3 µm^2)
60
50
40
30
20
10
0
***
***
***
***
30
30
30
7 6 5 4
B
V- MF5
V- MF6
I
C
R_in (MΩ)
20
15
10
5
0
***
***
***
**
37
38
41
27
7 6 5 4
τ_m (ms)
40
30
20
10
0
***
***
***
***
7 6 5 4
RMP (mV)
-80
-60
-40
-20
0
***
***
***
7 6 5 4